Structural Engineering and Mechanics, Vol. 20, No. 4 (2005) 405-420
DOI: http://dx.doi.org/10.12989/sem.2005.20.4.405

Efficient geometric nonlinear analyses of circular plate bending problems

Mei Duan†

School of Civil and Environmental Engineering, The University of New South Wales, Sydney, NSW 2052, Australia

(Received October 10, 2003, Revised October 14, 2004, Accepted April 11, 2005)

Abstract. In this paper, a hybrid/mixed nonlinear shell element is developed in polar coordinate system based on Hellinger/Reissner variational principle and the large-deflection theory of plate. A numerical solution scheme is formulated using the hybrid/mixed finite element method (HMFEM), in which the nodal values of bending moments and the deflection are the unknown discrete parameters. Stability of the present element is studied. The large-deflection analyses are performed for simple supported and clamped circular plates under uniformly distributed and concentrated loads using HMFEM and the traditional displacement finite element method. A parametric study is also conducted in the research. The accuracy of the shell element is investigated using numerical computations. Comparisons of numerical solutions are made with theoretical results, finite element analysis and the available numerical results. Excellent agreements are shown.

Key words: circular plate; geometric nonlinear; hybrid/mixed finite element.

1. Introduction

In the analysis of circular or annular plates, it is much more convenient to use polar coordinate system than rectangular Cartesian coordinate system. Circular plates have wide application in civil and mechanical engineering fields, such as the deformation of loading on foundations (Khathlan 1994) and the large-deflection analysis of glass plates (Vallabhan 1994). It was found that thin window-glass plates undergo large-deflections of ten times their thickness before they are failed by brittle fracture. Hence, it was necessary for a complete elastic, large-deflection analysis of glass plates to assess the behavior and design of thin-glass plates. The large-deflection analyses of circular plates bending under rectangular Cartesian coordinate system have been presented. Hong (1999) described a finite element method for the large-deflection analysis of axisymmetric shells and plates on a nonlinear tensionless elastic foundation. Takezono (1980) analyzed the elasto/viscoplastic behavior of thin circular plates under large strains using the finite element method based on the membrane shell theory. Generally, the obtained numerical solutions for circular plates agreed fairly well with the experimentally determined values. Michiya (1993) analyzed a uniformly loaded circular plate with a clamped edge based on a three-dimensional finite deformation theory, while Kondo and Pian (1981) analyzed the changes in geometry of the studied structures. Dumir (1987)

† Research Fellow, E-mail: mei@civeng.unsw.edu.au

considered the clamped and simply-supported plates with radially movable and fixed edges, analyzing the geometrically nonlinear, axisymmetric static and transient response of cylindrically orthotropic thin circular plates, resting on Pasternak elastic foundations subjected to uniformly distributed loads. Earlier, Dumir and Shingal (1986) were concerned with the geometrically nonlinear axisymmetric static and transient analysis of the moderately thick, cylindrically orthotropic circular plates subjected to uniformly distributed load and discrete central load. The analysis of shear deformation and rotary inertia was presented. Krayterman and Fu (1985) used the integral collocation method (ICM) to analyze the large deflected circular plates with clamped radially held and not held outer edge under uniform pressure. Turvey and Salehi (1997) implemented elastic large deflection analysis using dynamic relaxation algorithm.

HMFEM is one of multifield finite element methods that were originated by Pian (1964) to compensate for the shortages in the traditional finite element method. An excellent review above hybrid/mixed finite element researches was presented by Pian (1996). Hitoshi (1980) proposed a formulation of the mixed finite element method and applied a plane triangular element to the large-deflection analysis of the circular plate problem. Most of the researches, however, which were implemented under polar coordinate system, were about small deformation analysis, while majority of the large-deflection analyses were carried out under the rectangular coordinate system. There have been only a few investigations of the nonlinear analysis of circular plate bending using a polar coordinate system. This is mainly because the problems of a polar coordinate system can be transformed and carried out under a rectangular Cartesian system. However, the nonlinear behaviour is often dependent on the geometry of a structure and the applied load. As the error of domain approximation is ignored, see Fig. 1, a refinement element is necessary in the numerical analysis in order to achieve a high accuracy solution.

In this paper, a new element in the polar coordinates was suggested. The geometric nonlinear analysis of circular plate bending was performed using HMFEM. The incremental form of Hellinger/Reissner variational principle proposed by Pian (1976) was used to investigate simply supported and clamped circular plates under uniform loading conditions. The method employed to account for the elastic deformations was discussed. This research was an extension of a small-deflection analysis for the circular plate bending problem (Duan 1998). Numerical results were compared with theoretical solutions and those obtained by other researchers.

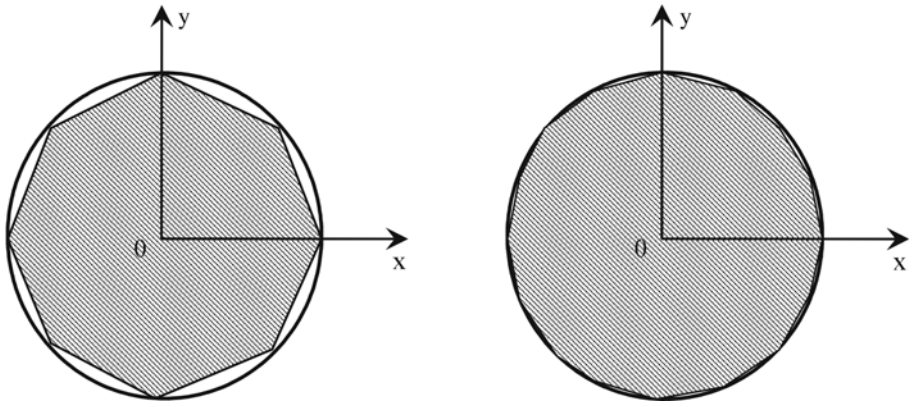

Fig. 1 Approximation of analysis domain under Cartesian coordinate system

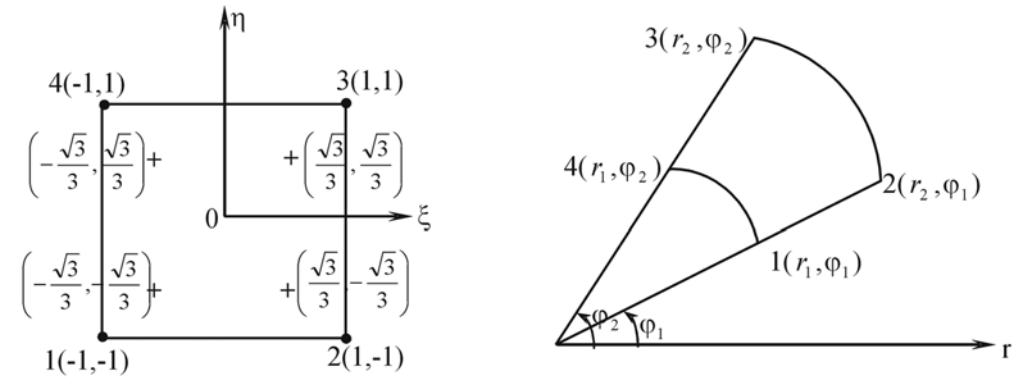

(a) Local Cartesian coordinate system (b) Polar coordinate system

Fig. 2 Coordinate system of element

2. Shell element

The positive directions of in-plane forces N_r, N_φ and $N_{r\varphi}$, bending moments M_r, M_φ and $M_{r\varphi}$, and transverse shear forces Q_r and Q_φ in polar coordinates are defined in Fig. 3. Based on the theory of circular plate bending (Szilard 1974), the in-plane forces, bending moments and transverse shear forces can be written as:

$$\begin{cases} N_r = \int_{-h/2}^{+h/2} \sigma_r dz \\ N_\varphi = \int_{-h/2}^{+h/2} \sigma_\varphi dz \\ N_{r\varphi} = \int_{-h/2}^{+h/2} \tau_{r\varphi} dz \end{cases}, \quad \begin{cases} M_r = \int_{-h/2}^{+h/2} \sigma_r z dz \\ M_\varphi = \int_{-h/2}^{+h/2} \sigma_\varphi z dz \\ M_{r\varphi} = \int_{-h/2}^{+h/2} \tau_{r\varphi} z dz \end{cases}, \quad \begin{cases} Q_r = \int_{-h/2}^{+h/2} \tau_{zr} dz \\ Q_\varphi = \int_{-h/2}^{+h/2} \tau_{z\varphi} dz \end{cases} \tag{1}$$

where σ_r, σ_φ, $\tau_{r\varphi}$, τ_{zr} and $\tau_{z\varphi}$ are the surface stress components.

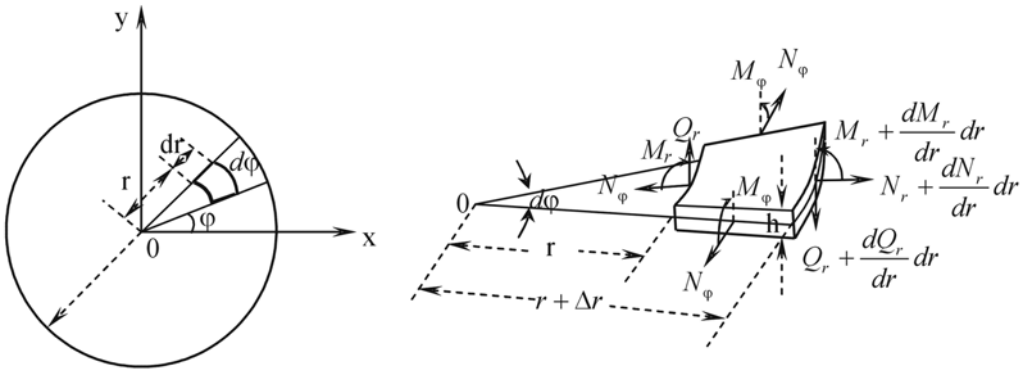

Fig. 3 Directions of tensile forces, bending moments and shearing forces for circular plate

The strain and displacement relationships for large deflection circular plate can be written as:

$$\begin{cases} \varepsilon_r = \dfrac{\partial u_r}{\partial r} + \dfrac{1}{2}\left(\dfrac{\partial w}{\partial r}\right)^2 \\ \varepsilon_\varphi = \dfrac{1}{r}\left(u_r + \dfrac{\partial u_\varphi}{\partial \varphi}\right) + \dfrac{1}{2r^2}\left(\dfrac{\partial w}{\partial \varphi}\right)^2 \\ \gamma_{r\varphi} = \dfrac{1}{r}\left(\dfrac{\partial u_r}{\partial \varphi} - u_\varphi\right) + \dfrac{\partial u_\varphi}{\partial r} + \dfrac{1}{r}\left(\dfrac{\partial w}{\partial r}\right)\left(\dfrac{\partial w}{\partial \varphi}\right) \end{cases} \tag{2}$$

where r and φ are the polar coordinates of circular plate, ε_r, ε_φ and $\gamma_{r\varphi}$ are strains in the radial and tangential directions and the shearing strain in the middle plane. u_r and u_φ are the in-plane displacements, and w is the deflection of plate.

The plate constitutive equations for isotropic materials are written as:

$$\begin{cases} N_r = \dfrac{Eh}{1-\upsilon^2}(\varepsilon_r + \upsilon\varepsilon_\varphi) \\ N_\varphi = \dfrac{Eh}{1-\upsilon^2}(\upsilon\varepsilon_r + \varepsilon_\varphi) \\ N_{r\varphi} = G\varepsilon_{r\varphi} \\ M_r = -D\left[\dfrac{\partial^2 w}{\partial r^2} + \upsilon\left(\dfrac{1}{r^2}\dfrac{\partial^2 w}{\partial \varphi^2} + \dfrac{1}{r}\dfrac{\partial w}{\partial r}\right)\right] \\ M_\varphi = -D\left[\upsilon\dfrac{\partial^2 w}{\partial r^2} + \left(\dfrac{1}{r^2}\dfrac{\partial^2 w}{\partial \varphi^2} + \dfrac{1}{r}\dfrac{\partial w}{\partial r}\right)\right] \\ M_{r\varphi} = (1-\upsilon)D\left(-\dfrac{1}{r}\dfrac{\partial^2 w}{\partial r\,\partial \varphi} + \dfrac{1}{r^2}\dfrac{\partial w}{\partial \varphi}\right) \\ Q_r = -D\dfrac{\partial}{\partial r}(\nabla_r{}^2 w) \\ Q_\varphi = -\dfrac{D}{r}\dfrac{\partial}{\partial \varphi}(\nabla_r{}^2 w) \end{cases} \tag{3}$$

where E, υ, h, $G = \dfrac{1}{2(1+\upsilon)}$, $D = \dfrac{Eh^3}{12(1-\upsilon^2)}$ and $\nabla_r^2 = \dfrac{\partial^2}{\partial r^2} + \dfrac{1}{r^2}\dfrac{\partial^2}{\partial \varphi^2} + \dfrac{1}{r}\dfrac{\partial}{\partial r}$ are Young's modulus, Poisson's ratio, the plate thickness, the shear modulus, the bending rigidity and the differential operator.

Thus, the governing differential equation can be obtained from Eqs. (2) and (3),

$$\begin{cases} \dfrac{D}{h}\nabla_r^2\nabla_r^2 w(r,\varphi) = \dfrac{\partial^2 w}{\partial r^2}\left(\dfrac{1}{r}\dfrac{\partial \Phi}{\partial r} + \dfrac{1}{r^2}\dfrac{\partial^2 \Phi}{\partial \varphi^2}\right) + \left(\dfrac{1}{r}\dfrac{\partial w}{\partial r} + \dfrac{1}{r^2}\dfrac{\partial^2 w}{\partial \varphi^2}\right)\dfrac{\partial^2 \Phi}{\partial r^2} - 2\dfrac{\partial}{\partial r}\left(\dfrac{1}{r}\dfrac{\partial \Phi}{\partial \varphi}\right)\dfrac{\partial}{\partial r}\left(\dfrac{1}{r}\dfrac{\partial w}{\partial \varphi}\right) + \dfrac{q}{h} \\ \dfrac{1}{E}\nabla_r^2\nabla_r^2 \Phi(r,\varphi) = \left(\dfrac{1}{r}\dfrac{\partial^2 w}{\partial r\,\partial \varphi} - \dfrac{1}{r^2}\dfrac{\partial w}{\partial \varphi}\right)^2 - \dfrac{1}{r}\dfrac{\partial^2 w}{\partial r^2}\dfrac{\partial w}{\partial r} - \dfrac{1}{r^2}\dfrac{\partial^2 w}{\partial r^2}\dfrac{\partial^2 w}{\partial^2 \varphi} \end{cases} \tag{4}$$

This is a nonlinear partial-differential equation of fourth order for r and φ.

Boundary Conditions:
$$\boldsymbol{T}^0 + \Delta\boldsymbol{T} = \overline{\boldsymbol{T}}^0 + \Delta\overline{\boldsymbol{T}} \quad \text{on} \quad \boldsymbol{S}_\sigma \tag{5}$$

$$\boldsymbol{u}^0 + \Delta\boldsymbol{u} = \overline{\boldsymbol{u}}^0 + \Delta\overline{\boldsymbol{u}} \quad \text{on} \quad \boldsymbol{S}_u \tag{6}$$

Based on the incremental form of Hellinger/Reissner variational principle (Pian 1976):

$$\pi_R(\Delta\boldsymbol{u}, \Delta\boldsymbol{\sigma}) = \sum_n \Bigg\{ \int_{V_n} -\frac{1}{2}\Delta\boldsymbol{\sigma}^T\boldsymbol{S}\Delta\boldsymbol{\sigma} + \boldsymbol{\sigma}^{0^T}(\boldsymbol{D}\Delta\boldsymbol{u}) - \overline{\boldsymbol{F}}^{0^T}\Delta\boldsymbol{u} - [(\boldsymbol{D}^T\Delta\boldsymbol{\sigma})^T + \Delta\overline{\boldsymbol{F}}^T]\Delta\boldsymbol{u} -$$

$$(\boldsymbol{D}^T\Delta\boldsymbol{\sigma})^T\boldsymbol{u}^0 - \Delta\boldsymbol{\sigma}^T\boldsymbol{\varepsilon}^0\}\,d\boldsymbol{V} - \int_{S_{\sigma_n}} [(\overline{\boldsymbol{T}}^{0^T} + \Delta\overline{\boldsymbol{T}}^T - \Delta\boldsymbol{T}^T)\Delta\boldsymbol{u} - \Delta\boldsymbol{T}^T\boldsymbol{u}^0]\,d\boldsymbol{S} +$$

$$\int_{S_{u_n}} [\Delta\boldsymbol{T}^T(\Delta\overline{\boldsymbol{u}} + \overline{\boldsymbol{u}}^0) - \boldsymbol{T}^{0^T}\Delta\boldsymbol{u}]\,d\boldsymbol{S} \Bigg\} \tag{7}$$

where $\boldsymbol{\sigma}^0, \boldsymbol{\varepsilon}^0, \boldsymbol{u}^0, \overline{\boldsymbol{F}}_i^0$ and $\boldsymbol{T}^0$ are initial stress, strain, displacement, body force components and initial surface traction. $\Delta\boldsymbol{\sigma}, \Delta\boldsymbol{\varepsilon}, \Delta\boldsymbol{u}, \Delta\overline{\boldsymbol{F}}$ and $\Delta\boldsymbol{T}$ are incremental stress, strain, displacement, body force components and incremental surface traction. S_{σ_n} and S_{u_n} are surfaces upon which traction vectors are employed and described for the nth element, and V_n is volume. $\boldsymbol{D}$ and $\boldsymbol{S}$ are differential operator matrix and material stiffness components, respectively.

Let
$$\Delta\boldsymbol{u} = \Delta\boldsymbol{u}_q + \Delta\boldsymbol{u}_\lambda \tag{8}$$

where $\Delta\boldsymbol{u}_q = \boldsymbol{N}(\Delta\boldsymbol{q})$ and $\Delta\boldsymbol{u}_\lambda = \boldsymbol{Z}(\Delta\lambda)$ are incremental compatible and incompatible displacement vectors.

Thus, making use of Eq. (8), $\pi_R(\Delta\boldsymbol{u}, \Delta\boldsymbol{\sigma})$ can be written as:

$$\pi_R(\Delta\boldsymbol{q}, \Delta\boldsymbol{\sigma}, \Delta\lambda) = \sum_n \Bigg\{ \int_{V_n} -\frac{1}{2}\Delta\boldsymbol{\sigma}^T\boldsymbol{S}\Delta\boldsymbol{\sigma} + \boldsymbol{\sigma}^{0^T}[\boldsymbol{D}(\boldsymbol{N}\Delta\boldsymbol{q} + \boldsymbol{Z}\Delta\lambda)] - \overline{\boldsymbol{F}}^{0^T}(\boldsymbol{N}\Delta\boldsymbol{q} + \boldsymbol{Z}\Delta\lambda) -$$

$$[(\boldsymbol{D}^T\Delta\boldsymbol{\sigma})^T + \Delta\overline{\boldsymbol{F}}^T](\boldsymbol{N}\Delta\boldsymbol{q} + \boldsymbol{Z}\Delta\lambda) - (\boldsymbol{D}^T\Delta\boldsymbol{\sigma})^T\boldsymbol{u}^0 - \Delta\boldsymbol{\sigma}^T\boldsymbol{\varepsilon}^0 \Big\} d\boldsymbol{V} -$$

$$\int_{S_{\sigma_n}} [(\overline{\boldsymbol{T}}^{0^T} + \Delta\overline{\boldsymbol{T}}^T - \Delta\boldsymbol{T}^T)(\boldsymbol{N}\Delta\boldsymbol{q} + \boldsymbol{Z}\Delta\lambda) - \Delta\boldsymbol{T}^T\boldsymbol{u}^0]\,d\boldsymbol{S} + \int_{S_{u_n}} [\Delta\boldsymbol{T}^T(\Delta\overline{\boldsymbol{u}} + \overline{\boldsymbol{u}}^0) - \boldsymbol{T}^{0^T}(\boldsymbol{N}\Delta\boldsymbol{q} + \boldsymbol{Z}\Delta\lambda)]\,d\boldsymbol{S} \Bigg\} \tag{9}$$

Assuming the incremental stress component $\Delta\boldsymbol{\sigma}$ as

$$\Delta\boldsymbol{\sigma} = \boldsymbol{P}\Delta\boldsymbol{\beta} \tag{10}$$

where $\boldsymbol{P}$ and $\Delta\boldsymbol{\beta}$ are stress function and parameter vector of incremental stress.

Substituting Eq. (10) into Eq. (9), in terms of $\Delta\boldsymbol{q}$, $\Delta\lambda$ and $\Delta\boldsymbol{\beta}$, the variational function π_R is expressed as:

$$\pi_R(\Delta \boldsymbol{q}, \Delta \boldsymbol{\beta}, \Delta \boldsymbol{\lambda}) = \sum_n \left\{ \int_{V_n} -\frac{1}{2}\Delta \boldsymbol{\beta}^T \boldsymbol{H} \Delta \boldsymbol{\beta} + \Delta \boldsymbol{\beta}^T \boldsymbol{G} \Delta \boldsymbol{q} - \Delta \boldsymbol{\beta}^T \boldsymbol{R} \Delta \boldsymbol{\lambda} + (\Delta \boldsymbol{Q} + \boldsymbol{R}^{\sigma} + \boldsymbol{R}^{\varepsilon}) \Delta \boldsymbol{q} \right\} \tag{11}$$

in where $\Delta \boldsymbol{Q}$, $\boldsymbol{R}^{\sigma}$ and $\boldsymbol{R}^{\varepsilon}$ are incremental nodal forces from the applied loads and nodal forces. $\boldsymbol{H}$, $\boldsymbol{G}$ and $\boldsymbol{R}$ are the flexibility and leverage matrices defined respectively by,

$$\boldsymbol{H} = \int_{V_n} \boldsymbol{P}^T \boldsymbol{S} \boldsymbol{P} dV, \qquad \boldsymbol{G} = \int_{V_n} \boldsymbol{P}^T \boldsymbol{C} (\boldsymbol{D}\boldsymbol{N}) dV, \qquad \boldsymbol{R} = \int_{V_n} (\boldsymbol{D}^T \boldsymbol{P})^T \boldsymbol{Z} dV$$

Taking variation of the variation function π_R with respect to parameter vectors, the following equation is obtained

$$\boldsymbol{K}^{(e)} \Delta \boldsymbol{q} = \Delta \boldsymbol{Q} + \boldsymbol{R}^{\sigma} + \boldsymbol{R}^{\varepsilon} \tag{12}$$

in which the element stiffness matrix $\boldsymbol{K}^{(e)}$ is expressed as

$$\boldsymbol{K}^{(e)} = \tilde{\boldsymbol{G}}^T \boldsymbol{H}^{-1} \tilde{\boldsymbol{G}}, \qquad \tilde{\boldsymbol{G}} = \boldsymbol{G} - \boldsymbol{R} (\boldsymbol{R}^T \boldsymbol{H}^{-1} \boldsymbol{R})^{-1} \boldsymbol{R}^T \boldsymbol{H}^{-1} \boldsymbol{G}$$

3. Hybrid/mixed finite element analysis in the polar coordinates

In this paper, a four-nodal nonlinear hybrid/mixed circular plate element with five degrees of freedom at each node is proposed. Three translations (u, v, w) along x, y and z directions and two rotations (θ_1, θ_2) are formulated in the current research. We assume the incremental displacement vectors as

$$\Delta \boldsymbol{u}_q = \boldsymbol{N} \Delta \boldsymbol{q} \qquad \text{and} \qquad \Delta \boldsymbol{u}_{\lambda} = \boldsymbol{I}_2 \Delta \boldsymbol{\lambda} \tag{13}$$

where $\Delta \boldsymbol{u}_q = \{\Delta u, \Delta v, \Delta w, \Delta \theta_1, \Delta \theta_2\}$ and $\boldsymbol{N} = [N_1 I_4, N_2 I_4, N_3 I_4, N_4 I_4]$. $\Delta \boldsymbol{q}$ and $\Delta \boldsymbol{\lambda} = \{\Delta \lambda_1, \Delta \lambda_2\}$ are incremental node displacement and parameter vector, respectively. The shape functions N_i (i = 1, 2, 3, 4) are written as $N_i = \frac{1}{4}(1 + \xi_i \xi)(1 + \eta_i \eta)$ (i = 1, 2, 3, 4) and $\boldsymbol{I_i}$ denotes the ith-order identity matrix.

The incremental stress $\boldsymbol{\sigma} = \{N_r, N_{\varphi}, N_{r\varphi}, M_r, M_{\varphi}, M_{r\varphi}, Q_r, Q_{\varphi}\}^T$ is defined as

$$\Delta \boldsymbol{\sigma} = \begin{Bmatrix} \Delta \boldsymbol{M}_1 \\ \Delta \boldsymbol{M}_2 \end{Bmatrix}, \qquad \Delta \boldsymbol{M}_1 = \begin{bmatrix} 1 & 0 & 0 & \eta & 0 \\ 0 & 1 & 0 & 0 & \xi \\ 0 & 0 & 1 & 0 & 0 \end{bmatrix} \Delta \boldsymbol{\beta}_1 \quad \text{and}$$

$$\Delta \boldsymbol{M}_2 = \begin{bmatrix} 1 & 0 & 0 & \xi & \eta & 0 & 0 & 0 & 0 & \xi\eta & 0 \\ 0 & 1 & 0 & 0 & 0 & \xi & \eta & 0 & 0 & 0 & \xi\eta \\ 0 & 0 & 1 & 0 & 0 & 0 & 0 & \xi & \eta & 0 & 0 \\ 0 & 0 & 0 & 1 & 0 & 0 & 0 & 0 & 1 & \eta & 0 \\ 0 & 0 & 0 & 0 & 0 & 0 & 1 & 1 & 0 & 0 & \xi \end{bmatrix} \Delta \boldsymbol{\beta}_2 \tag{14}$$

where stress parameters $\boldsymbol{\beta}_1$ and $\boldsymbol{\beta}_2$ are expressed as $\boldsymbol{\beta}_1 = \{\beta_1, \beta_2, \beta_3, \beta_4, \beta_5\}^T$ and $\boldsymbol{\beta}_2 = \{\beta_6, \beta_7, \beta_8, \beta_9, \beta_{10}, \beta_{11}, \beta_{12}, \beta_{13}, \beta_{14}, \beta_{15}, \beta_{16}\}^T$, respectively.

The geometric mapping relations of local Cartesian coordinate system and polar coordinate system as shown in Fig. 2 can be written as:

$$\begin{cases} r = \dfrac{r_1 + r_2}{2} + \dfrac{r_2 - r_1}{2}\eta \\ \varphi = \dfrac{\varphi_1 + \varphi_2}{2} + \dfrac{\varphi_2 - \varphi_1}{2}\xi \end{cases} \qquad (\varphi_1 \neq \varphi_2, r_1 \neq r_2) \tag{15}$$

in which (r, φ) and (ξ, η) are polar coordinate system and local Cartesian coordinate system, respectively. The sampling points of integration functions are shown in Fig. 2(a).

We note that

$$\begin{vmatrix} \dfrac{\partial r}{\partial \xi} & \dfrac{\partial r}{\partial \eta} \\ \dfrac{\partial \varphi}{\partial \xi} & \dfrac{\partial \varphi}{\partial \eta} \end{vmatrix} \neq 0 \tag{16}$$

is nonsingular. Then the geometric mapping relations (Eq. (15)) is invertible.

$$\begin{cases} \dfrac{\partial N_i}{\partial r} = \dfrac{\partial N_i}{\partial \xi}\dfrac{\partial \xi}{\partial r} + \dfrac{\partial N_i}{\partial \eta}\dfrac{\partial \eta}{\partial r} = \dfrac{\eta_i}{2(r_2 - r_1)}(1 + \xi_i \xi) \\ \dfrac{\partial N_i}{\partial \varphi} = \dfrac{\partial N_i}{\partial \xi}\dfrac{\partial \xi}{\partial \varphi} + \dfrac{\partial N_i}{\partial \eta}\dfrac{\partial \eta}{\partial \varphi} = \dfrac{\xi_i}{2(r_2 - r_1)}(1 + \eta_i \eta) \end{cases} \qquad (i = 1, 2, 3, 4) \tag{17}$$

4. Stability investigate

In this section, the stability of solution in thin plate limit was investigated. The Babuska-Brezzi stability condition (Babusa 1973) can be written as:

$$\begin{cases} n_M \geq n_\theta - 3 \\ n_s \geq n_w - 1 \\ n_M + n_s \geq n_\theta + n_w - 3 \end{cases} \tag{18}$$

where n_M, n_θ, n_s and n_w are the number of variables of bending moments, rotations, shear forces and vertical displacement in the element.

The hybrid/mixed shell element with $n_M = 11$, $n_\theta = 8$, $n_s = 6$ and $n_w = 4$ shows that it has no spurious modes. When the inf-sup condition is considered based on Bathe's research (2001), the smallest nonzero eigenvalue $\lambda_{\min}$ of the present shell element stably changes in the neighborhood of 10^{-3} for thin ~ thick plates as the number of meshes is increased. It is seen that the element passes the inf-sup test and has no shear locking.

5. Numerical applications

According to the theoretical formulation presented in Section 2, numerical analyses were performed for various types of loading and boundary conditions using HMFEM. The obtained numerical results were compared with the theoretical results and other available numerical results.

5.1 Clamped circular plate

A circular plate bending problem with clamped edges was analyzed for geometrically nonlinear behavior under dimensionless uniform loading using hybrid/mixed shell element. The relevant model is shown in Fig. 4. Because of symmetry, only a quarter of the circular plate was investigated

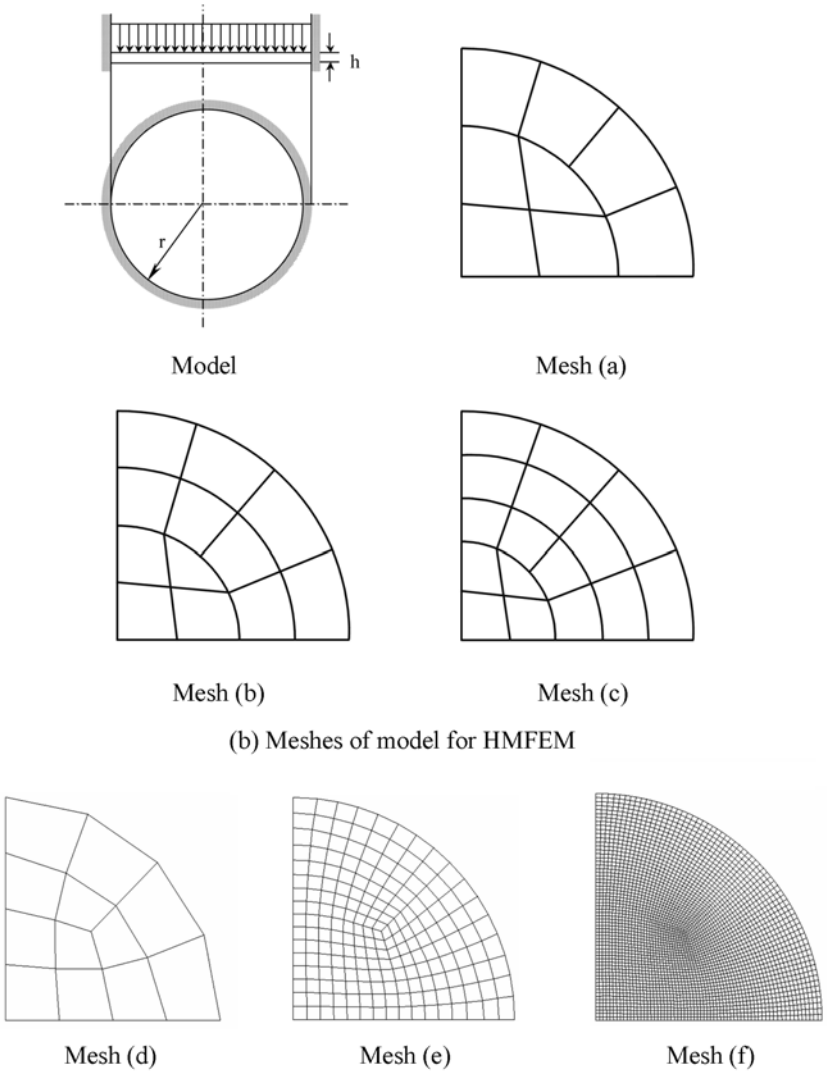

Fig. 4 Circular plate model and meshes

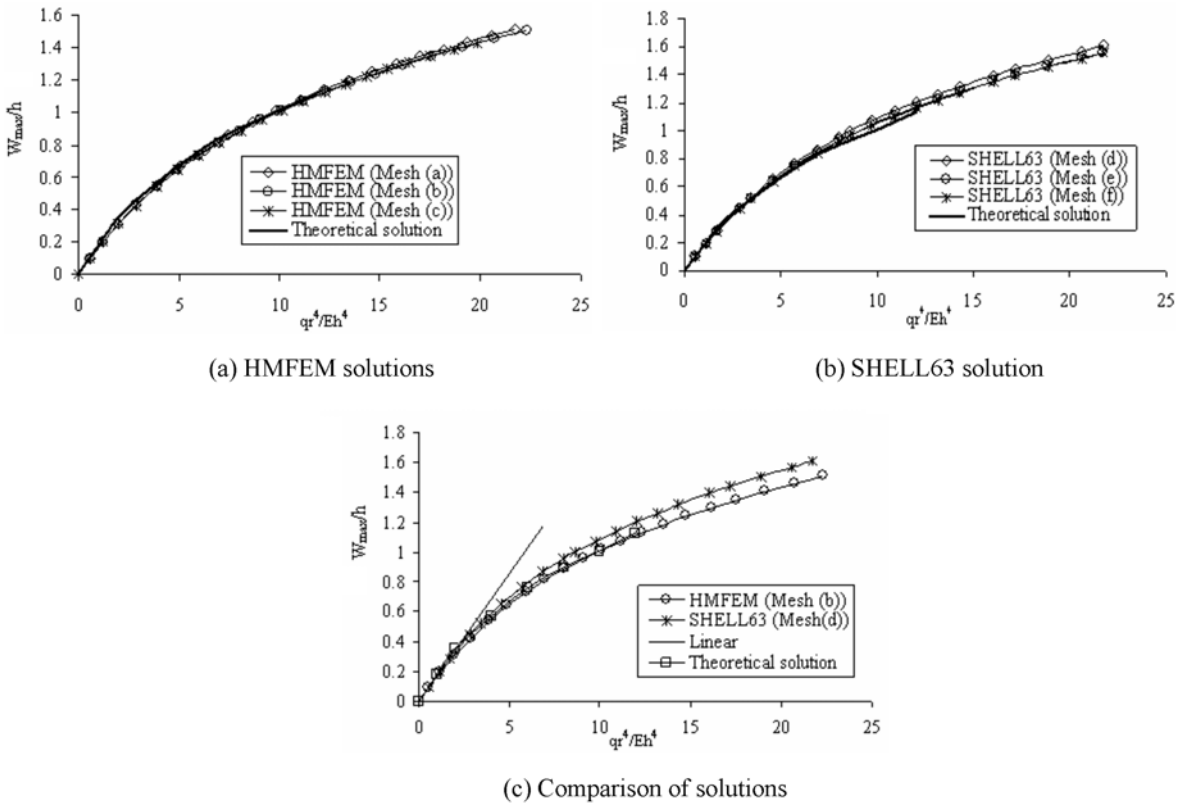

(a) HMFEM solutions

(b) SHELL63 solution

(c) Comparison of solutions

Fig. 5 Load-deflection curves for circular plate bending

and meshes were divided, as shown in Fig. 4. The value of Poisson's ratio $\upsilon = 0.3$ and a ratio of $h/r = 0.02$ were used in the analysis. The results of HMFEM using mesh (a), mesh (b) and mesh (c), numerical results from 4-node quadrilateral shell element (SHELL63) of ANSYS analysis program using mesh (d), mesh (e) and mesh (f) (Kohnke 1998), linear solution and nonlinear reference theory solutions (Timoshenko and Woinowsky-Krieger 1959) are shown in Fig. 5. From the comparison of results, it is clear that the results of HMFEM that converge to theoretical solution are considered accurate even for a relatively coarse mesh. However, element SHELL63 uses over 20 times element numbers and degree-of-freedom numbers than the present hybrid/mixed shell element to obtain the same accuracy. This implies that present element cannot only improve the accuracy of solution, but also save analysis time when the same accuracy is required.

In this section, three different values of Poisson's ratio, i.e., $\upsilon = 0.25$, 0.30, 0.35 were used in the analysis for a plate with ratio $h/a = 0.02$. Mesh (c) of the model shown in Fig. 4 was employed and values of $\upsilon = 0.3$ and $h/r = 0.02$ were implemented in the analysis. The numerical results of HMFEM using mesh (c) and reference theory solution (Timoshenko and Woinowsky-Krieger 1959) are compared, as shown in Fig. 6. The numerical results indicate that the solutions of HMFEM are accurate. The numerical results obtained in this analysis agree well with the theoretical values. It is clear that the present hybrid/mixed shell element is also suitable for using in other structural materials except all structural steels.

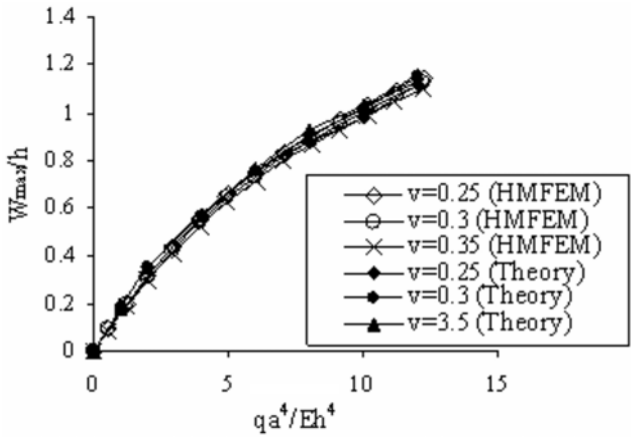

Fig. 6 Load-deflection curves for circular plates with different Poisson's ratios

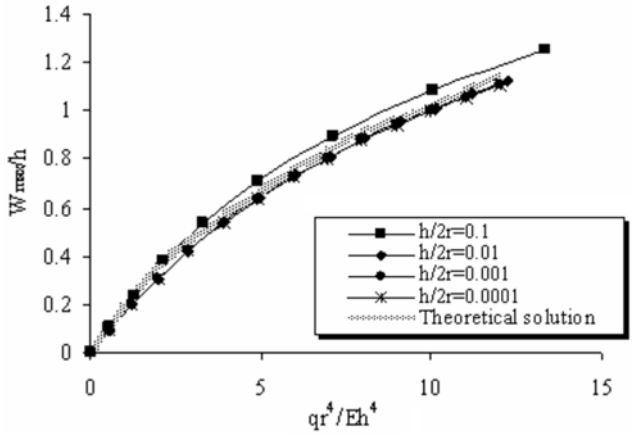

Fig. 7 Comparison of load-deflection curves for thin ~ thick circular plates

The deflection curves for different values of the thickness-to-diameter ratio $h/2r$ are shown in Fig. 7. A comprehensive analysis of the uniformly loaded circular plates with clamped and hinged boundary conditions was given and the effects of all governing parameters, including the ratio of plate radius-to-thickness r/h were discussed. It is clear that the dimensionless load deflection is independent of the $h/2r$ ratio unless it is a thick plate. The results of HMFEM plotted in Fig. 7 also show that the large-deflections of plates are less sensitive to $h/2r$ and that the present hybrid/mixed element has no shear locking phenomenon.

5.2 Circular plate subjected to partially distributed load

In this section, the large-deflection problem of the circular plate was analyzed for clamped edge condition under partially uniformly distributed and concentrated loads using the present hybrid/mixed shell element. The relevant model is shown in Fig. 8. The radiuses of the circular plate and the distributed load over inner circle are R and r, respectively. Because of symmetry of structure and

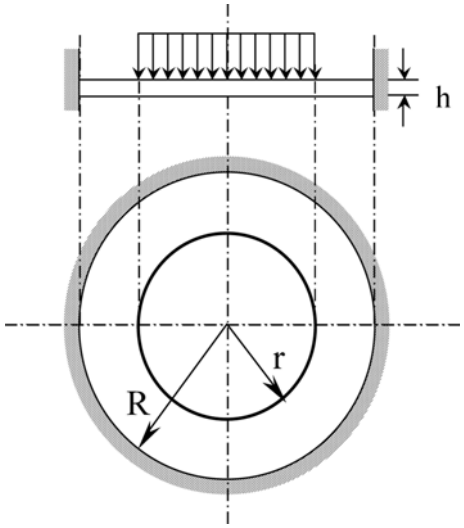

Fig. 8 Circular plate under partially distributed load

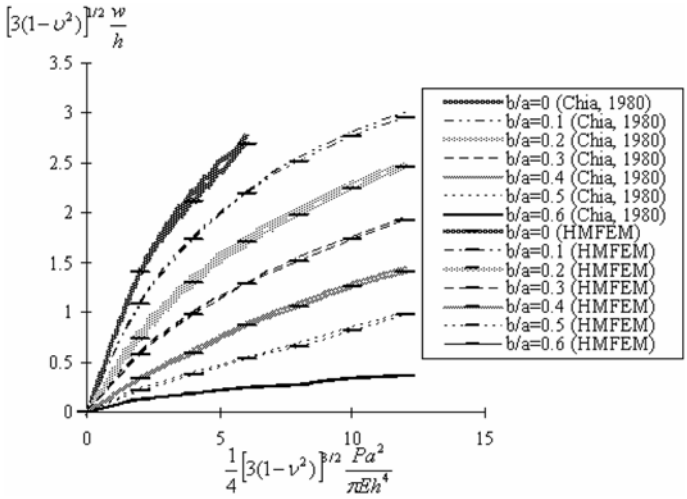

Fig. 9 Comparison of solutions for clamped plate under partially distributed load

load, only a quarter of the circular plate was investigated in the numerical analysis. Values of $\upsilon = 0.3$ and $h/r = 0.02$ were implemented using the present shell element under the polar coordinate system. The circular plates subjected to different loadings ratios with $r/R = 0$~0.6 were studied. In particular, $r/R = 0$ expresses that a concentrated load is subjected. The accuracy of solution was investigated and the load-deflection curves of the circular plate were plotted and compared with reference theory solutions (Chia 1980), as shown in Fig. 9. It is seen that the different loads have a greater effect on the large deflection of the circular plate and the largest deflection is shown for the case of concentrated load. The analysis results obtained using HMFEM agree well with theoretical solutions for all cases including uniform distributed and concentrated loads.

5.3 Simply supported circular plate

A circular plate bending problem with simply supported edges was analyzed for geometrically nonlinear behavior under uniform loading using HMFEM. The model is shown in Fig. 10. Poisson's ratio, $\upsilon = 0.25$, 0.30, 0.35 and $h/r = 0.02$ were performed in the analysis. The numerical results of HMFEM and reference theory solution (Stippes and Hausrath 1952) were compared and shown in Fig. 11. It is clear that a good agreement of the numerical solutions was also obtained for the simply supported circular plate. The numerical analysis of HMFEM further shows that it can also be used for all structural steels and other structural materials.

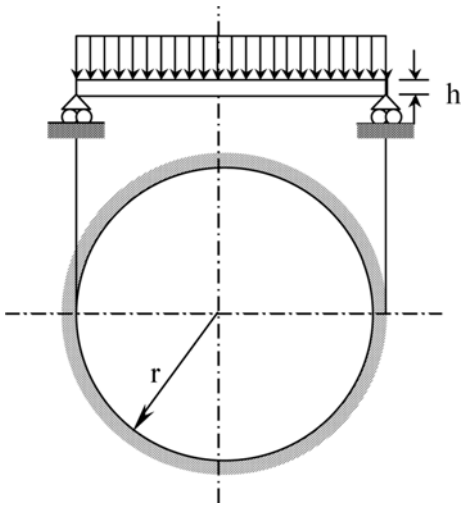

Fig. 10 Simply supported circular plate

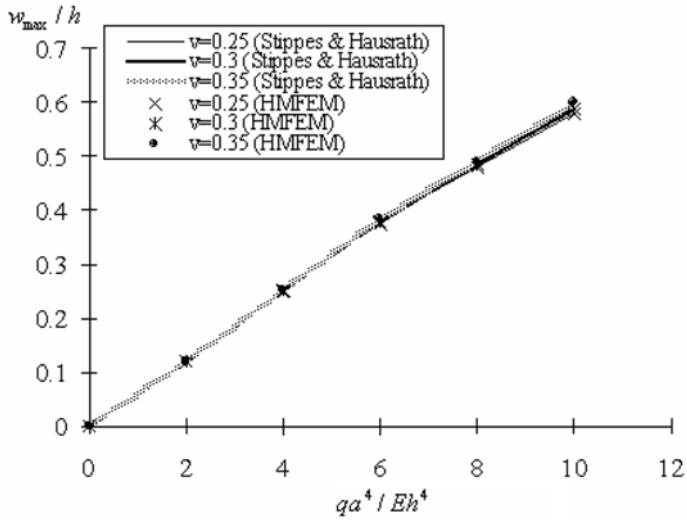

Fig. 11 Load-deflection curves of simply supported plate

5.4 Ellipse plate

In the preceding section, the circular plates with clamped and simply supported boundary conditions and uniformly distributed, partially distributed and concentrated loads were discussed. Furthermore, an ellipse plate under a uniformly distributed load, as shown in Fig. 12, was also investigated. As a representative study, the ellipse plate with a/b = 0.5 ratio was considered in the

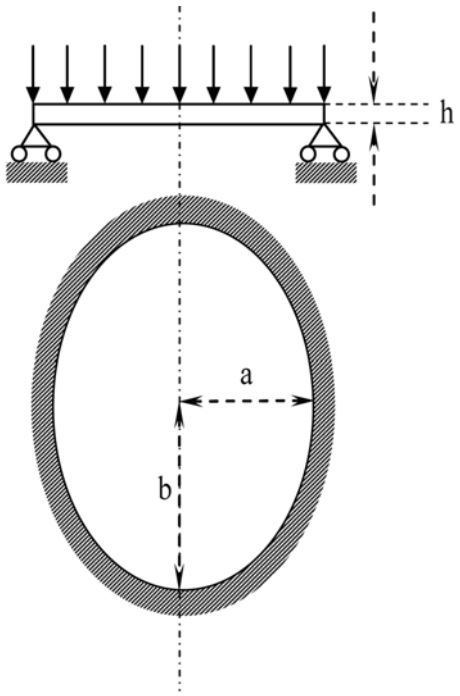

Fig. 12 Ellipse plate under uniform load

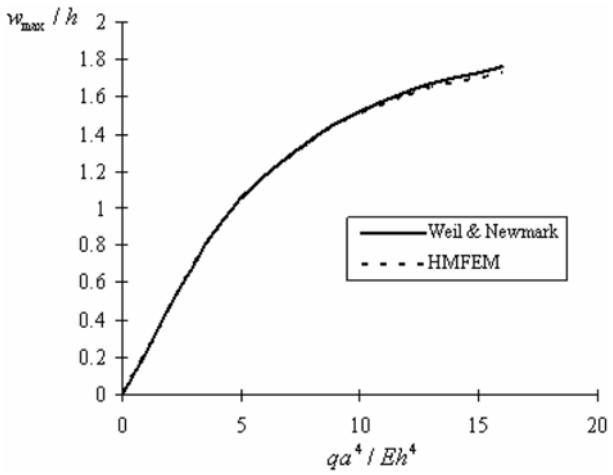

Fig. 13 Load-deflection curves of ellipse plate

analysis. The numerical results of large deflection were obtained and compared with previously published results (Well and Newmark 1956), as shown in Fig. 13. An excellent agreement was achieved. By comparing the results of circular plate shown in Fig. 5, it is seen that the different shape of ellipse plates have an effect on the large deflection of the ellipse plate.

5.5 Annular plate subjected to line force

Above all analyses have shown that the high accurate results have been obtained using the presented analysis method. In order to exhibit that the method is also efficient for any load cases, an annular plate subjected to line force is investigated, as shown in Fig. 14. Young's modulus of 21×10^6, Poisson's ratio of 0.0, thickness of 0.03, outer radius of 10 and internal radius of 6 are employed in the analysis. The meshes of 3×12 shown in Fig. 14 are implemented in the analysis using HMFEM. The numerical solutions are presented and compared with the reference solution (Sansour and Kollmann 2000) in Fig. 15. It is seen that a good agreement is presented.

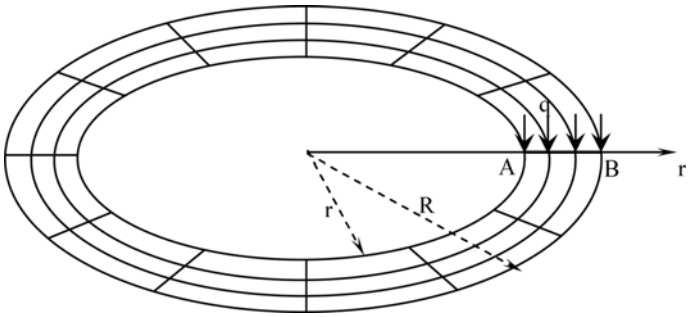

Fig. 14 Annular plate subjected to line force

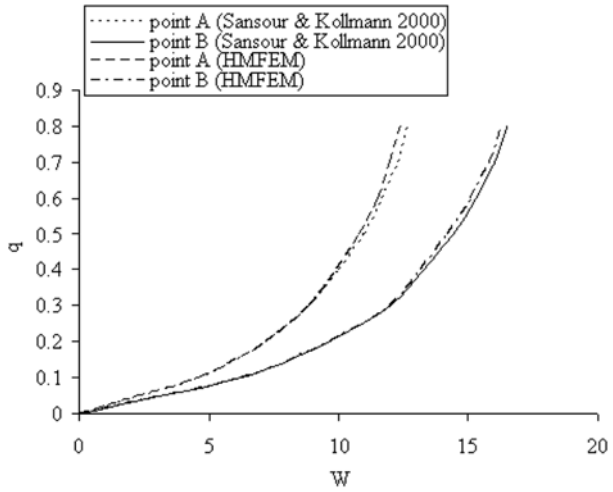

Fig. 15 Load-deflection curves of annular plate subjected to line force

6. Conclusions

In this paper, a hybrid/mixed nonlinear shell element was developed in polar coordinate system. Non-dimensional parametric and large-deflection analyses of circular plates were presented using HMFEM. Large-deformation behaviour of circular plates was assessed for various circular plates such as simply supported and clamped circular plates under full uniform or partly distributed uniform and concentrated loads. The non-linear characteristic relations concerning load and deflection factors were numerically analyzed and presented. The comparisons of numerical solutions with theoretical results and finite element analysis showed good agreements. It is seen that the present study provides an efficient analysis method for circular plate bending problems in structural engineering.

References

Babusa, I. (1973), "The finite element method with Largrange multipliers", *Numer. Math.*, **20**, 179-192.
Bathe, K.J. (2001), "The inf-sup condition and its evaluation for mixed finite element methods", *J. Comput. Struct.*, **79**, 243-252.
Chia, C.Y. (1980), *Nonlinear Analysis of Plates*, McGraw-Hill.
Duan, M., Miyamoto, Y., Iwasaki, S. and Deto, H. (1998), "Hybrid/mixed finite element analysis of circular plate bending based on Reissner-Mindlin theory", *J. of Structural and Construction Engineering (JSCE)*, **44A**, 323-330.
Dumir, P.C. (1987), "Circular plates on pasternak elastic foundations", *Int. J. Numer. Anal. Methods Geomech.,* **11**(1), 51-60.
Dumir, P.C. and Shingal, L. (1986), "Nonlinear analysis of thick circular plates", *J. Eng. Mech.,* **112**(3), 260-272.
Hitoshi, W. (1980), "Nonlinear analysis of plates and shells by the incremental procedure using a mixed model of the finite element method", *Bulletin of the JSME,* **23**(186), 1945-1951.
Hong, T. (1999), "Axisymmetric shells and plates on tensionless elastic foundations", *Int. J. Solids Struct.*, **36**(34), 5277-5300.
Khathlan, A.A. (1994), "Large-deformation analysis of plates on unilateral elastic foundation", *J. Eng. Mech.*, **120**(8), 1820-1827.
Kohnke, P. (1998), *Theory Manual*. Houston, PA. USA: ANSYS, Inc.
Kondo, K. and Pian, T.H.H. (1981) "Large deformations of rigid-plastic circular plates", *Int. J. Solids Struct.*, **17**(11), 1043-1055.
Krayterman, B.L. and Fu, C.C. (1985), "Nonlinear analysis of clamped circulars", *J. Struct. Eng.,* **111**(11), 2402-2415.
Michiya, K. (1993) "Strain analysis of 3-dimensional elastic large deformation for a thick circular plate by convected coordinates (comparison with the classical plate theory), Nippon Kikai Gakkai Ronbunshu", *A Hen/ Transactions of the Japan Society of Mechanical Engineers*, Part A, **59**(561), 1232-1237.
Pian, T.H.H. (1964), "Derivation of element stiffness matrices by assumed stress distributions", *AIAA* **7**, 1333-1335.
Pian, T.H.H. (1976), "Variational principle for incremental finite element methods", *Journal of The Franklin Institute*, **302**(5 & 6), 473-488.
Pian, T.H.H. (1996), "Survey of hybrid/mixed finite element methods for plate and shell analysis", *Third Asian-Pacific Conf. on Computational Mechanics*, 227-232.
Sansour, C. and Kollmann, F.G. (2000), "Families of 4-node and 9-node finite elements for a finite deformation shell theory", *Comput. Mech.*, **24**, 435-447.
Stippes, M. and Hausrath, A.H. (1952), "Large deflections of circular plates", *Trans. ASME, J. Appl. Mech.*, **19**, 187-292.
Szilard, R. (1974), *Theory and Analysis of Plates*, Prentice-Hall, INC. Englewood Cliffs, New Jersey.

Takezono, S. (1980), "Elasto/viscoplastic analysis of thin circular plates under large strains and large deformations", *J. Appl. Mech., Transactions ASME*, **47**(4), 741-747.
Timoshenko, S. and Woinowsky-Kreiger, S. (1959), *Theory of Plates and Shells*, McGraw-Hill New York.
Turvey, G.J. and Salehi, M. (1997), "Circular plates with one diametral stiffener – an elastic large deflection analysis", *Comput. Struct.*, **63**(4), 775-783.
Vallabhan, C.V. (1994), "Parametric study of axisymmetric circular-glass plates", *J. Struct. Eng.,* **120**(5), 1663-1671.
Well, N.A. and Newmark, N.M. (1956), "Large deflection of elliptical plates", *Trans. ASME, J. Appl. Mech.*, **23**, 21-26.